Long-wavelength instabilities in three-layer flow down an incline

Steven J. Weinstein and Mark R. Kurz
Emulsion Coating Technologies, Bldg. 35, Eastman Kodak Company, Rochester, New York 14652-3701

(Received 17 December 1990; accepted 15 July 1991)

This paper reports a long-wavelength instability which has not previously been identified for three-layer free-surface flow down an inclined plane. The instability is identified in the zeroth-order asymptotic solution in wave number, indicating that *neither* inertial nor finite wavelength effects are necessary to induce instabilities in three-layer systems. Various neutral stability boundaries are presented which demonstrate the effect of viscosity stratification, density stratification, and layer thicknesses. It is found that destabilization occurs in cases where the middle-layer viscosity (for equal densities in each layer) or density (for equal viscosities in each layer) is smaller than those of the adjacent layers. The regions of instability afford a smooth transition between neutrally stable regions of the parameter space where the in-phase and out-of-phase characteristics of the interfaces differ.

I. INTRODUCTION

It is well-known that the rectilinear flow of multiple fluid layers down an inclined plane can be unstable. These instabilities manifest themselves as waves which travel along the fluid interfaces, down the inclined plane in the direction of the bulk fluid flow. The predominant application of the inclined plane flow geometry is in the manufacture of multiple-layer products such as photographic films, where the inclined plane provides a means by which individual fluid layers can be stacked on top of one another. At the end of the plane, these layers are then deposited simultaneously on a moving substrate.

There has been much work done to determine the stability of single-layer Newtonian flows. The neutral stability of single-layer flows (for example, see Benjamin,[1] Binnie,[2] and Yih[3]) is characterized by a critical Reynolds number, $\mathrm{Re} = \rho Q/\mu$ (where ρ is the density, Q is the volumetric flow rate per unit width, and μ is the viscosity), for a given angle of inclination, β, beyond which waves will begin to grow. These results can be obtained by performing a long-wavelength asymptotic analysis on the equations governing the fluid flow (see Yih[3]), since instability appears to manifest itself at long wavelengths.

Kao[4–6] has investigated the long-wavelength stability of two-layer Newtonian systems, where the effects of viscosity and density stratification are discussed. Akhtaruzzaman *et al.*[7] investigated the long-wavelength motion of a three-layer system whose stability was subsequently determined by Wang *et al.*[8] These multiple-layer analyses show that the number of wave solutions is generally equal to the number of interfaces in the problem. One of the wave solutions has properties which are quite similar to those of the single-layer case (which will be called the surface mode) and persists in the limit as the fluid properties in each layer become equal. The other wave solutions owe their existence to the presence of the fluid–fluid interfaces in the problem (henceforth called interface modes). In these multiple-layer references, attention is restricted to long wavelengths, since it is presumed that instabilities manifest themselves at long wavelengths. Employing this postulate, a conclusion that might be drawn from these stability analyses is that inertial effects (characterized by the Reynolds number) are necessary to induce instability in both the surface and interface modes at long wavelengths. This is because the zeroth-order approximation in α (where α is the wave number) yields no information about wave growth, i.e., neutrally stable results are obtained; there is no inertia present to this order. It is only in the $O(\alpha)$ approximation, which incorporates inertial effects, that long-wavelength instabilities can be deduced.

Work by Loewenhurz and Lawrence[9] indicates that inertia is necessary to induce instabilities in the surface mode. They specifically investigated the case where the Reynolds number was identically zero, but did not restrict themselves to a long-wavelength approximation. They found that the surface mode solution is stable at zero Reynolds number for all finite wavelengths. This is in agreement with the single-layer and multiple-layer results cited previously, since this literature presumes that the system stability is determined at long wavelengths, and thus instabilities cannot exist for any wavelength. However, Loewenhurz and Lawrence[9] show that the interface mode *can be unstable* in the long-wavelength limit even when the Reynolds number is identically zero; in particular, when the top-layer viscosity is greater than the bottom-layer viscosity. In the limit as $\alpha \to 0$, however, one would have to retain terms to presumably $O(\alpha^2)$ or higher to deduce the instability (Loewenhurz and Lawrence[9] did not explicitly consider an asymptotic expansion), i.e., *finite* wavelength effects must be included. This is because the $O(\alpha)$ correction must be zero when there are no inertial terms, to be consistent with the previously cited work for multiple layers. Then, even at long wavelengths, interface mode instabilities can arise when there is no inertia.

As pointed out by Loewenhurz and Lawrence[9] and can be seen in the results of Weinstein,[10] for a given physical system, waves with the largest growth typically occur at finite wavelengths; the properties of these largest growing waves is often of most practical interest. However, to determine the spatial growth of waves at finite wavelengths for the general case that includes inertia, it is necessary to utilize accurate initial guesses (see Weinstein[10]). This is because there is a nonlinear eigenvalue problem to solve which has

 0899-8213/91/112680-08$02.00

more than one wave solution, i.e., the surface and interface modes. The long-wavelength solutions provide such initial guesses, and thus it is necessary to accurately characterize the long-wavelength limit.

This work reports a long-wavelength instability which has not previously been identified for *three-layer* flow down an inclined plane. Thus, it is an extension of the work of Akhtaruzzaman *et al.*,[7] who did not identify the instability. In contrast to the above cited cases, the reported instability is identified in the zeroth-order asymptotic solution, i.e., $O(1)$, where *neither* inertia nor finite wavelength effects are present. This instability is somewhat analogous to that reported by Li[11] for three-layer plane Couette flow. The three-layer instability reported in this paper can occur in cases where the middle-layer viscosity (for equal densities in each layer) or density (for equal viscosities in each layer) is smaller than those of the adjacent layers. The instability arises for these cases because the zeroth-order eigenvalue problem exhibits complex conjugate behavior, apparently owing to the presence of an additional interface (compared with the two-layer inclined plane flow, which does not exhibit such an instability). This additional interface affords the possibility that the wave solutions which owe their existence to the presence of the *interfaces* can "resonate" together, i.e., interact quite strongly (see Li[11]). As pointed out by Li,[11] Taylor[12] identified a resonating instability for three-layer inviscid flow where the top and bottom layers were of infinite extent; this instability was characterized by backward moving waves at the upper interface and forward moving waves at the lower interface, relative to the underlying fluid flow. The instability presented in the present work appears to have this character.

Before closing the introductory remarks, it is noted that the wave motion along the free surface cannot be neglected in an effort to simplify the stability analysis; this is despite the fact that it is the existence of interface modes which give rise to the instability discussed in this paper. Lin[13] examined the long-wavelength stability of two-layer flow down an incline where the free surface was assumed to be flat (a solidification problem was considered where the free surface solidified before the rest of the fluid) and was able to identify a zeroth-order instability. This is in contrast with the above-cited two-layer results, where no instability could be found in the zeroth-order solution. Thus, despite the fact that it is the presence of each interface and the free surface which allows for the existence of each interface mode and free-surface mode, the *whole* zeroth-order flow field affects each mode to a large extent (as discussed by Loewenhurz and Lawrence[9]).

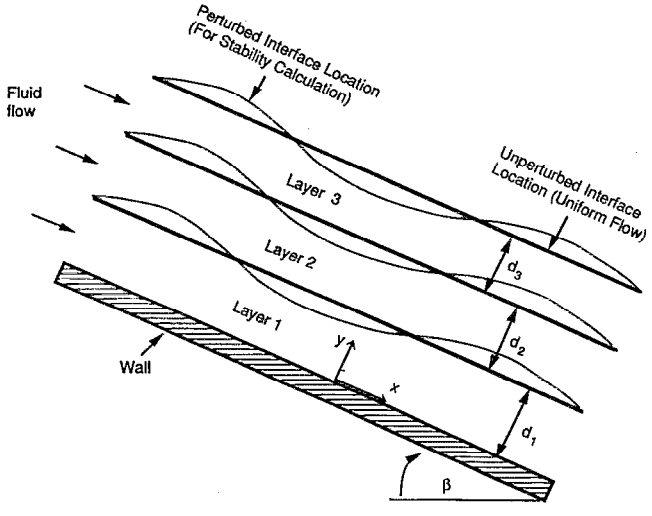

FIG. 1. The geometry of the uniform flow and stability problems.

The organization of this paper is as follows. In Sec. II, the equations governing the stability of uniform three-layer flow down an incline in the long-wavelength limit are obtained. In addition, cubic equations are explicitly obtained to determine wave growth for the case of viscosity stratification and for the case of density stratification. Results are presented in Sec. III, primarily in the form of neutral stability curves; these results are discussed in Sec. IV, and conclusions are given in Sec. V.

II. FORMULATION

The equations governing the stability of three-layer flow down an incline have been derived by Akhtaruzzaman *et al.*[7] Consequently, in this section we will highlight the important details of their analysis, reflecting the new notation that is used in this paper. To this end, consider the configuration shown in Fig. 1. Here, three layers of fluids with specified properties are flowing down an infinite plane inclined at angle β under the influence of gravity, g, where the thicknesses of each layer are specified. The fluid interfaces and free surface are all parallel to the solid inclined surface (hereafter called the wall), and the flow in each layer is everywhere parallel to the wall. Let the origin of an x-y coordinate system be placed at the wall, the y axis oriented toward the free surface and the x axis in the direction of flow. The bottom layer of the pack is denoted as layer 1, the second as layer 2, and the top as layer 3. It should be noted here that this is opposite to the convention used by Akhtaruzzaman *et al.*[7] We will refer to the fluid–fluid interface closest to the wall as the first interface, the next fluid–fluid interface as the second interface, and the air–fluid interface as the free surface. The viscosity, density, and thickness of each layer are denoted as μ_k, ρ_k, and d_k, respectively, where $k \in [1,3]$.

It is convenient to make variables dimensionless using d_T, the total thickness of the three-layer system, and Q_s, a volumetric flow scale defined as

$$Q_s = \rho_2 g d_T^3 \sin\beta / 2\mu_2 .$$

Thus $y \sim d_T$, while the velocity in each layer scales as $V_{x_k} \sim Q_s/d_T$. It turns out that the pressure in the uniform flow problem is hydrostatic and thus does not interact with the fluid flow. The choice for this pressure scale is made based on the dynamics of the stability problem to be considered subsequently; for convenience, the pressure is made dimensionless here as $P_k \sim \rho_k Q_s^2/d_T^2$. All dimensionless quantities will be denoted with an overbar.

Using these scales, the velocity solutions to the Navier–

Stokes equations are given by the following parabolic profiles:

$$\bar{V}_{x_k}(\bar{y}) = B_k \bar{y}^2 + C_k \bar{y} + D_k, \quad k \in [1,3], \tag{1a}$$

where

$$B_k = -R_k/E_k, \tag{1b}$$

$$C_k = \frac{2}{E_k}\left(R_k \sum_{n=1}^{k} \delta_n + \sum_{n=k+1}^{3} R_n \delta_n\right), \tag{1c}$$

$$D_k = \sum_{n=1}^{k-1}\left(\frac{R_{n+1}}{E_{n+1}} - \frac{R_n}{E_n}\right)\left(\sum_{m=1}^{n} \delta_m\right)^2 + \sum_{n=1}^{k-1}(C_n - C_{n+1}) \sum_{m=1}^{n} \delta_m, \tag{1d}$$

and

$$R_k = \frac{\rho_k}{\rho_2}, \quad E_k = \frac{\mu_k}{\mu_2}, \quad \delta_k = \frac{d_k}{d_T}. \tag{1e}$$

Then, the final functional dependence for $\bar{V}_{x_k}$ is given by

$$\bar{V}_{x_k} = \bar{V}_{x_k}(\bar{y}; \delta_1, \delta_3, R_1, R_3, E_1, E_3) \tag{1f}$$

and pressure in each layer is

$$\bar{P}_k = \frac{\bar{P}_A}{R_k} - \frac{2\cot\beta}{\mathrm{Re}_2}\left(\bar{y} - \sum_{n=1}^{k} \delta_n - \sum_{n=k+1}^{3} \frac{R_n \delta_n}{R_k}\right), \tag{1g}$$

where $\bar{P}_A \rho_2 Q_s^2/d_T^2$ is the atmospheric pressure and $\mathrm{Re}_2 = \rho_2 Q_s/\mu_2$. This completes the consideration of the uniform flow problem.

To assess the stability of the three-layer flow, the appropriate time-dependent governing equations and boundary conditions are linearized about (1). Then a streamfunction, $\bar{\psi}_k Q_s$, is defined, which removes the explicit appearance of the pressure in the linearized system, and an equivalent boundary-value problem which is only in terms of $\bar{\psi}_k$ is obtained. It is then seen that all solutions to the linearized equations can be written as the superposition of temporally growing waves whose translation is characterized by the location $\bar{x} d_T$ and time $\bar{t} d_T^2/Q_s$ as

$$\bar{\psi}_k = \phi_k(\bar{y}) e^{i\alpha(\bar{x} - c\bar{t})}. \tag{2a}$$

It is then necessary to determine the unknown functions $\phi_k(\bar{y})$ and the functionality $c(\alpha)$. In (2a), i denotes imaginary, α is the purely real wave number defined as $\alpha = 2\pi d_T/\lambda$ (λ is the wavelength), $c = c_R + ic_I$ is the complex wave speed, where the real part of c, denoted by c_R, gives the wave speed, and the imaginary part of c, denoted by c_I, determines the temporal growth or decay of waves along the inclined plane. It will be shown that the stability results for temporally growing waves are identical to those for spatially growing waves, to the order of the approximations used in this paper. Note that based on (2a), the deviation of each interface from its unperturbed location, $\bar{\zeta}_k d_T$, is then given by

$$\bar{\zeta}_k = \frac{\phi_k}{(c - \bar{V}_{x_k})} e^{i\alpha(\bar{x} - c\bar{t})} \quad \text{at } \bar{y} = \sum_{n=1}^{k} \delta_n. \tag{2b}$$

Employing (2a), the resulting system of equations is equivalent to Eqs. (i)–(iv) of Akhtaruzzaman *et al.*,[7] once appropriate notation changes are made:

governing equations:

$$\frac{d^4\phi_k}{d\bar{y}^4} - 2\alpha^2 \frac{d^2\phi_k}{d\bar{y}^2} + \alpha^4 \phi_k = -i\alpha\,\mathrm{Re}_2 \frac{R_k}{E_k}\left[\left(\frac{d^2\phi_k}{d\bar{y}^2} - \alpha^2\phi_k\right)(c - \bar{V}_{x_k}) + \phi_k \frac{d^2\bar{V}_{x_k}}{d\bar{y}^2}\right], \quad k \in [1,3]; \tag{3a}$$

boundary conditions at $\bar{y} = 0$:

$$\phi_1 = 0, \tag{3b}$$

$$\frac{d\phi_1}{d\bar{y}} = 0; \tag{3c}$$

boundary conditions at $\bar{y} = \Sigma_{n=1}^{k} \delta_n$:

$$\frac{d\phi_{k+1}}{d\bar{y}} = \frac{d\phi_k}{d\bar{y}} + \frac{\phi_k}{(c - \bar{V}_{x_k})}\left(\frac{d\bar{V}_{x_k}}{d\bar{y}} - \frac{d\bar{V}_{x_{k+1}}}{d\bar{y}}\right), \quad k \in [1,2], \tag{3d}$$

$$\phi_{k+1} = \phi_k, \quad k \in [1,2], \tag{3e}$$

$$E_k \frac{d^3\phi_k}{d\bar{y}^3} - E_{k+1}\frac{d^3\phi_{k+1}}{d\bar{y}^3} - 3\alpha^2\left(E_k \frac{d\phi_k}{d\bar{y}} - E_{k+1}\frac{d\phi_{k+1}}{d\bar{y}}\right) + i\alpha\,\mathrm{Re}_2(c - \bar{V}_{x_k})\left(R_k \frac{d\phi_k}{d\bar{y}} - R_{k+1}\frac{d\phi_{k+1}}{d\bar{y}}\right) + i\alpha\,\mathrm{Re}_2\,\phi_k\left(R_k \frac{d\bar{V}_{x_k}}{d\bar{y}} - R_{k+1} \times \frac{d\bar{V}_{x_{k+1}}}{d\bar{y}}\right) - \frac{\phi_k}{(c - \bar{V}_{x_k})}\left(2i\alpha(R_k - R_{k+1})\cot\beta + \frac{i\alpha^3}{\mathrm{Ca}_k}\right) = 0, \quad k \in [1,3], \tag{3f}$$

$$E_{k+1}\left(\frac{d^2\phi_{k+1}}{d\bar{y}^2} + \alpha^2\phi_{k+1}\right) - E_k\left(\frac{d^2\phi_k}{d\bar{y}^2} + \alpha^2\phi_k\right) - 2(R_{k+1} - R_k)\frac{\phi_k}{(c - \bar{V}_{x_k})} = 0, \quad k \in [1,3], \tag{3g}$$

where $E_4 = R_4 = \phi_4 = 0$, $\bar{V}_{x_k}$ is given by (1), and $\mathrm{Ca}_k^{-1} = \sigma_k d_T/\mu_2 Q_s$ is a capillary number in terms of the constant surface tension of each interface, σ_k. The boundary-value problem (3) constitutes a homogeneous system of equations and boundary conditions, i.e., it is an eigenvalue problem to determine the complex wave speed c as a function of α for given physical, geometrical, and flow properties as

$$c = c(\alpha, \delta_1, \delta_3, R_1, R_3, E_1, E_3, \cot\beta, \mathrm{Re}_2, \mathrm{Ca}_1, \mathrm{Ca}_2, \mathrm{Ca}_3).$$

Corresponding complex eigenfunctions are given by (2).

In the long-wavelength limit, i.e., $\alpha \to 0$, the complex wave speed and eigenfunctions are expanded as

$$c \sim c_0(\delta_1, \delta_3, R_1, R_3, E_1, E_3, \cot\beta, \mathrm{Re}_2, \mathrm{Ca}_1, \mathrm{Ca}_2, \mathrm{Ca}_3) + O(\alpha),$$

$$\phi_k \sim \phi_{k_0}(\bar{y}; \delta_1, \delta_3, R_1, R_3, E_1, E_3, \cot\beta, \mathrm{Re}_2, \mathrm{Ca}_1, \mathrm{Ca}_2, \mathrm{Ca}_3) + O(\alpha),$$

where the subscript (0) denotes zeroth order in α. These ex-

pansions are substituted into the governing equations (3), and a set of simplified equations, valid in the $\alpha \to 0$ limit is obtained. In this paper, we consider only the zeroth-order approximation; note that in what follows, the functions ϕ_k are presented without the subscript (0), but they are understood to be lowest order. The resulting system of equations is

governing equations:

$$\frac{d^4\phi_k}{d\bar{y}^4} = 0, \quad k \in [1,3]; \tag{4a}$$

boundary conditions at $\bar{y} = 0$:

$$\phi_1 = 0, \tag{4b}$$

$$\frac{d\phi_1}{d\bar{y}} = 0; \tag{4c}$$

boundary conditions at $\bar{y} = \Sigma_{n=1}^{k} \delta_n$:

$$\frac{d\phi_{k+1}}{d\bar{y}} = \frac{d\phi_k}{d\bar{y}} + \frac{\phi_k}{(c_0 - \bar{V}_{x_k})}\left(\frac{d\bar{V}_{x_k}}{d\bar{y}} - \frac{d\bar{V}_{x_{k+1}}}{d\bar{y}}\right), \quad \text{for } k \in [1,2], \tag{4d}$$

$$\phi_{k+1} = \phi_k, \quad \text{for } k \in [1,2], \tag{4e}$$

$$E_k \frac{d^3\phi_k}{d\bar{y}^3} - E_{k+1}\frac{d^3\phi_{k+1}}{d\bar{y}^3} = 0, \quad \text{for } k \in [1,3], \tag{4f}$$

$$E_{k+1}\frac{d^2\phi_{k+1}}{d\bar{y}^2} - E_k \frac{d^2\phi_k}{d\bar{y}^2} - 2(R_{k+1} - R_k) \times \frac{\phi_k}{(c_0 - \bar{V}_{x_k})} = 0, \quad \text{for } k \in [1,3]. \tag{4g}$$

Again, note that $E_4 = R_4 = \phi_4 = 0$. The system (4) is identical to that of Akhtaruzzaman *et al.*,[7] once appropriate notation changes are made.

By inspection of the simplified system (4) it is thus clear that

$$c_0 = c_0(\delta_1, \delta_3, R_1, R_3, E_1, E_3), \tag{5}$$

where in general $c_0 = c_{0_R} + ic_{0_I}$. Note that (5) indicates that the lowest-order complex wave speed is not a function of wave number, i.e., the system is nondispersive. Consequently, the temporal and spatial formulations of the problem yield identical stability results at this order.[14] In the lowest-order approximation, temporal wave growth is quantified by the following exponential term taken from (2):

$$\text{growth} = e^{\alpha c_{0_I} \bar{t}}. \tag{6}$$

From (6), it is clear that when $\alpha c_{0_I} > 0$, the flow is unstable, and for $\alpha c_{0_I} < 0$, the flow is stable. Then $c_{0_I} = 0$ in (5) determines the functionality in the parameter space which borders on instability, i.e., neutral stability is determined.

The characteristic equation (5) to solve for c_0 can be obtained analytically. In order to focus on the specific roles of viscosity and density stratification, these cases are considered separately in this paper. For purposes of simplicity, two characteristic equations are obtained: one for systems where there is viscosity stratification but no density stratification ($R_1 = R_3 = 1$), and the second for systems where there is density stratification but no viscosity stratification ($E_1 = E_3 = 1$). For either of these cases, the resulting equation is cubic:

$$c_0^3 + a_2 c_0^2 + a_1 c_0 + a_0 = 0, \tag{7}$$

where it is understood that the coefficients are different for the density and viscosity stratification cases. The details of the calculations leading to (7), as well as the definition of the coefficients, are give in the Appendix. It is important to note that the coefficients in (7) are real, where the roots of the cubic equation are characterized by the following trial function:

$$L = q^3 + r^2, \tag{8a}$$

where

$$q = \frac{a_1}{3} - \frac{a_2^2}{9}, \quad r = \frac{1}{6}(a_1 a_2 - 3a_0) - \frac{a_2^3}{27}. \tag{8b}$$

In solving the cubic, instabilities arise if there is one real root and two complex conjugate roots, which occurs when $L > 0$ in (8a). For this case, the complex wave speeds become

$$c_0 = -\frac{1}{2}(U_1 + U_2) - \frac{a_2}{3} \pm \frac{i\sqrt{3}}{2}(U_1 - U_2), \tag{8c}$$

$$c_0 = U_1 + U_2 - (a_2/3), \tag{8d}$$

where

$$U_1 = \sqrt{r + \sqrt{L}}, \quad U_2 = \sqrt{r - \sqrt{L}}. \tag{8e}$$

From (8c), it is clear that the neutral condition for the complex conjugate solutions corresponds to a case where the conjugates collapse onto the real axis, and at least two of the roots are equal; thus, the neutral stability condition for complex conjugates reduces to

$$L = q^3 + r^2 = 0, \tag{9}$$

which is parametrized in (5) with $c_{0_I} = 0$. Note that for $L < 0$, all the roots of (7) are real.

Restricting attention to the unstable interface mode given by (8c), the amplitudes, A_k, and phases, θ_k, of the interfaces induced by this mode relative to those of the first interface can be written, using (2b), as

$$A_k/A_1 = \|\phi_k(c_0 - \bar{V}_{x_1})/\phi_1(c_0 - \bar{V}_{x_k})\|, \quad k \in [2,3], \tag{10a}$$

$$\theta_k - \theta_1 = \tan^{-1}\left[\frac{\text{Im}[\phi_k(c_0 - \bar{V}_{x_1})/\phi_1(c_0 - \bar{V}_{x_k})]}{\text{Re}[\phi_k(c_0 - \bar{V}_{x_1})/\phi_1(c_0 - \bar{V}_{x_k})]}\right], \quad k \in [2,3], \tag{10b}$$

where the ϕ_k and $\bar{V}_{x_k}$ values are all interpreted as being evaluated at the respective interfaces, where $k = 1$ corresponds to the first interface, $k = 2$ corresponds to the second interface, and $k = 3$ corresponds to the free surface. In (10a) the symbol $\|F\|$ denotes the magnitude of the general complex argument F, while in (10b) the notation Im and Re denote the imaginary and real parts of the arguments.

We end this section by noting that condition (9) yields a boundary between the *region of instability* and the *region of neutral stability* in the zeroth-order approximation. This is because for cases where $L < 0$, the zeroth-order approximation yields only neutrally stable results. Consequently, (9) is not a neutral stability condition in the usual sense, since waves do not go from a state of growth to a state of damping upon traversing the boundary described by (9); by contrast, in this work, waves go from a state of growth to that of neutral stability upon traversing the boundary.

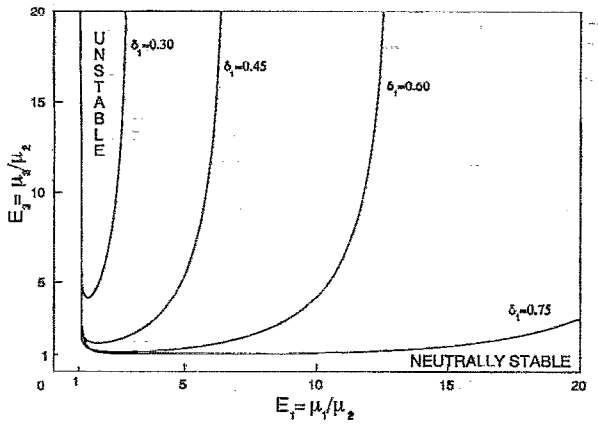

FIG. 2. The effect of middle-layer placement on instability regions for various viscosity ratios, where $\delta_2 = 0.1$.

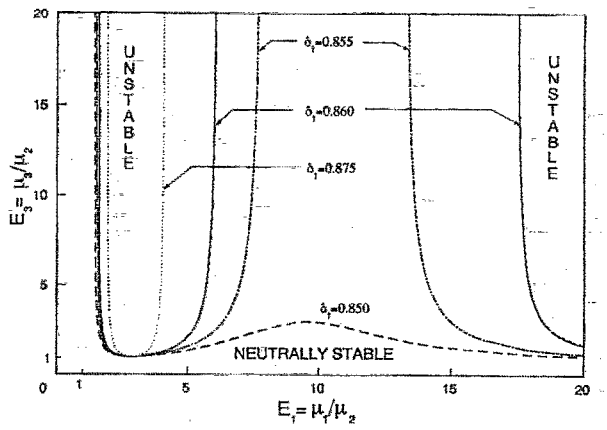

FIG. 3. The effect of middle-layer placement on instability regions for various viscosity ratios, where $\delta_2 = 0.1$, and $\delta_1 > 0.85$.

III. RESULTS

We begin this section by assigning a physical significance to the wave modes given by (8c) and (8d). In the limit as all the fluid layer properties become equal, it is straightforward to show that the wave solution given by (8d) smoothly limits to the surface wave found in single-layer flow down an incline (see Yih[3]). For this reason we denote this wave solution as the surface mode. Note that this mode is always neutrally stable in the zeroth-order approximation, which is consistent with the previously cited literature results in the Introduction. In this same limit, the wave solutions given by (8c) are neutrally stable, where their speeds are identical to that of the uniform flow at each of the two interfaces. For this reason, we denote these modes as interface modes, which clearly owe their existence to the presence of the interfaces in the problem when fluid properties are not the same in the layers. Then, in the zeroth-order approximation, it is the *interface* modes which can exhibit instabilities according to (8c). For more details regarding the properties of the surface and interface modes, see Weinstein.[10] Note that the limits just described have been used to check the correctness of the cubic equation given by (7).

We now examine the parametric conditions under which interface mode instabilities in the three-layer flow can arise, via the neutral stability condition given by (9). Figures 2 and 3 show the effect of moving a middle layer of constant thickness away from the wall, for cases of viscosity stratification where $E_1, E_3 \in [0,20]$ (and $R_1 = R_3 = 1$). It is apparent that instabilities can only arise if the middle-layer viscosity is smaller than those of the two adjacent layers; this behavior was seen for all viscosity stratification cases surveyed. Note that our calculations indicate that the line $E_1 = 1$ in Figs. 2 and 3 is often extremely close to the neutral stability boundary and is sometimes numerically indistinguishable; however, as Fig. 3 clearly indicates, the line $E_1 = 1$ typically is *not* a neutral stability boundary, although it always lies in a neutrally stable region. In Fig. 2, it is seen that as the bottom layer becomes thinner, the region of instability decreases in size. For these results, when the bottom-layer thickness is decreased below approximately $\delta_1 = 0.22$ (not shown on the plot), no region of instability arises for the viscosity ratios considered. Figure 3 indicates the effect of increasing the bottom-layer thickness past $\delta_1 = 0.75$, i.e., decreasing the thickness of the top layer. It is seen that the neutral stability contours radically change their shapes compared with the cases of Fig. 2; Fig. 3 shows that the regions of instability diminish in size in the limit as $\delta_3 \to 0$. Note also that we have also considered viscosity ratios larger than $E_3 = 20$, and as $E_3 \to \infty$, the regions of instability in Figs. 2 and 3 persist. By inspection of the coefficients of (7) given in (A2), it is clear that in the limit as $E_3 \to \infty$ the coefficients of the cubic equation are not functions of E_3, indicating that the roots of the cubic are insensitive to E_3 in this limit. Then, if complex conjugate behavior is exhibited for finite but large values of E_3, this behavior will extend to infinity. Mathematically speaking, this accounts for the vertical lines to which the neutral stability boundaries asymptote in Figs. 2 and 3 as $E_3 \to \infty$.

Figures 4(a) and 4(b) indicate how the relative phases and amplitudes of the free surface and the interfaces, given by (10), vary as a function of E_1 for the unstable interface mode, where $\delta_1 = 0.6$, $\delta_2 = 0.1$, and $E_3 = 5$; this corresponds to traversing the line $E_3 = 5$ in Fig. 2, for $E_1 \in [1,10.5]$. The reference phase and amplitude for these results are taken to be those for the bottom interface. In Fig. 4(a), it is seen that as $E_1 \to 1$, the free surface and bottom interface are in phase, while the bottom interface and middle interface are $-180°$ out of phase; note that the relative phases vary extremely rapidly with E_1 as $E_1 \to 1$. On the other hand, as $E_1 \to 10.5$, all of the interfaces are oscillating in phase. It is thus seen that the region of instability affords a smooth transition between the in-phase and out-of-phase regions of the parameter space. In Fig. 4(b) it is seen that as $E_1 \to 1$, the middle interface and free surface have extremely small amplitudes relative to the bottom interface, which is assigned a relative amplitude of 1, i.e., the bottom interface is most largely affected by the unstable interface mode (note that the relative amplitudes for $E_1 \approx 1$ are small but nonzero; this is not apparent due to the scale of the figure). As $E_1 \to 10.5$, it is apparent that all three interfaces are largely affected by the unstable interface mode.

For the same conditions as Figs. 4(a) and 4(b), Fig. 4(c) shows the speed of the complex conjugate interface modes relative to that of the unperturbed free surface and interface speeds.

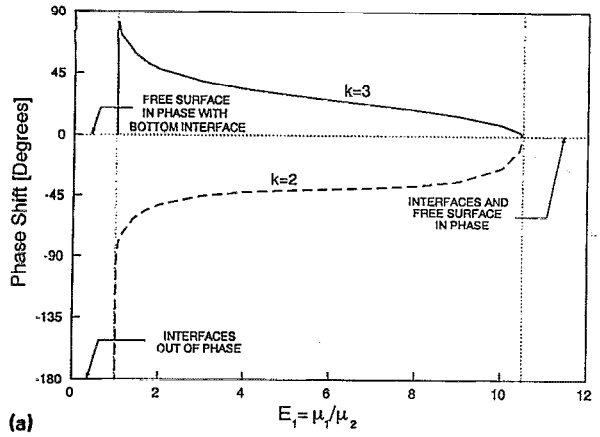

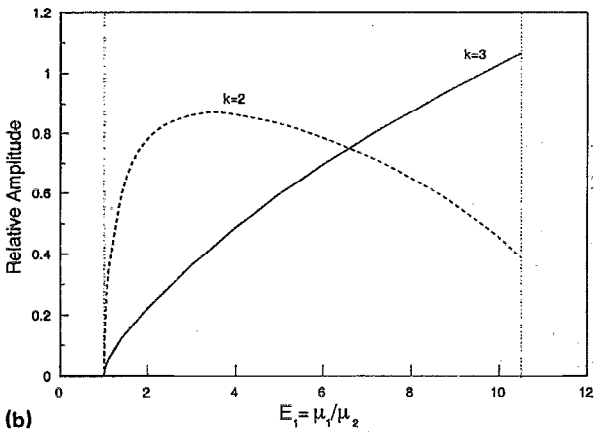

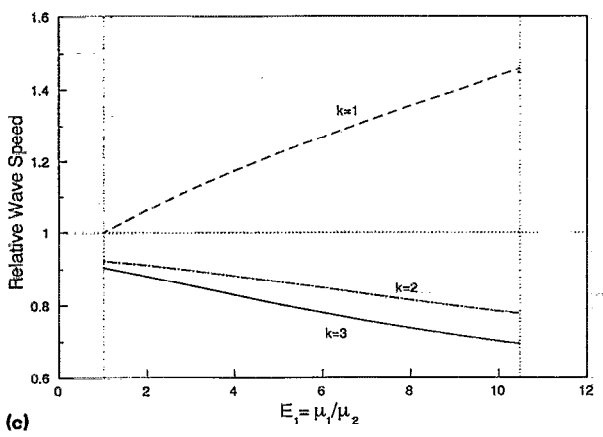

FIG. 4. The effect of the unstable interface mode on (a) the phase shift at the second interface and free surface relative to that of the first interface ($\theta_k - \theta_1$), and (b) the amplitudes of the second interface and free surface relative to that of the bottom interface (A_k/A_1). (c) The wave speed of the unstable interface mode relative to the unperturbed fluid velocities [Real$(c_0)/\overline{V}_{x_k}$] at the first interface ($k=1$), second interface ($k=2$), and free surface ($k=3$).

Note that the wave speed is larger than the corresponding unperturbed fluid speed at the first interface, but it is smaller than the unperturbed fluid speed at the second interface and free surface. Note also that as $E_1 \to 10.5$, the relative interfacial wave-speed curves become farther apart. The divergence of these relative interface curves as E_1 is increased appears to correlate with the recovery of neutral stability. Further, note that as $E_1 \to 1$, the wave speed of the interface mode relative to the speed of the fluid at the unperturbed interface approaches 1; this is a manifestation of the fact that a two-layer system is obtained, where the interface no longer represents a boundary between physically distinct layers.

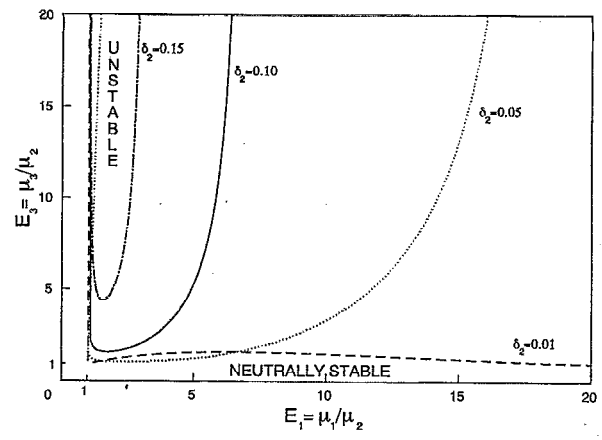

FIG. 5. The effect of the middle-layer thickness on instability regions for various viscosity ratios, where $\delta_1 = \delta_3$.

Figure 5 demonstrates the effect of viscosity ratios, while increasing the thickness of the middle layer and reducing the thickness of the other two layers, where $\delta_1 = \delta_3$. It is seen that as the middle layer increases in thickness, the region of instability diminishes in size. In fact, for δ_2 greater than approximately 0.18, no region of instability can be found for $E_1, E_3 \in [0,20]$. Note also that for $\delta_2 = 0.01$, the neutral stability curve is similar in shape to the $\delta_1 = 0.85$ curve of Fig. 3. For $\delta_2 < 0.01$ in Fig. 5 (not shown), a radical change in the stability diagram occurs as was seen in Fig. 3. As was done for cases shown in Figs. 2 and 3, we have considered viscosity ratios larger than $E_3 = 20$, and as $E_3 \to \infty$, the regions of instability in Fig. 5 persist.

Finally, we consider the effect of density stratification on the neutral stability diagram. Figure 6 gives results for $R_1, R_3 \in [0,20]$ (and $E_1 = E_3 = 1$), for the case where the mid-

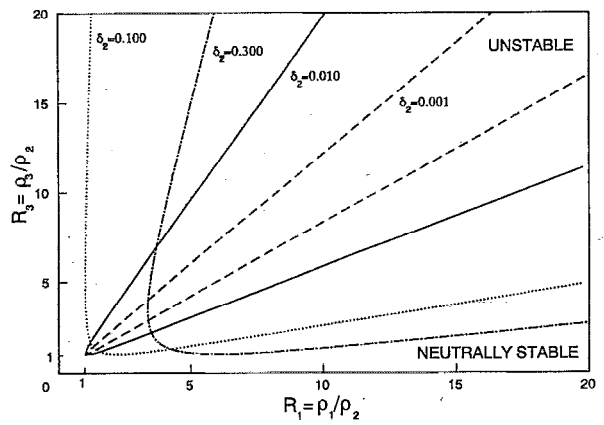

FIG. 6. The effect of the middle-layer thickness on instability regions for various density ratios, where $\delta_1 = \delta_3$.

dle-layer thickness is increased, while decreasing the thickness of the other two layers where $\delta_1 = \delta_3$. For all the cases surveyed, we were able to find instabilities only for cases where the middle-layer density is smaller than those of the two adjacent layers. Note that it is seen that as the middle-layer thickness is increased, from $\delta_2 = 0.001$, the size of the window first increases; however, between $\delta_2 \in [0.1, 0.3]$, the instability region begins to shift to higher values of R_1. Note also that as $\delta_2 \to 0$, the region of instability appears to diminish in size and eventually disappears in the limit. Our calculations also indicate that each of the regions shown persists in the limit as $R_1 \to \infty$ and $R_3 \to \infty$.

IV. DISCUSSION

We begin our discussion by noting the consistency of our three-layer neutral stability contours with the two-layer results cited in the Introduction. For cases of viscosity stratification, Figs. 2, 3, and 5 all indicate that the systems with $E_1 = 1$ or $E_3 = 1$ are neutrally stable in the zeroth-order approximation in α; these are two-layer systems that do not exhibit complex conjugate behavior (see Kao[6] and Loewenhurz and Lawrence[9]). Figure 2 indicates that as the thickness of the top layer decreases, the regions of instability diminish in size, which indicates that in the limit of zero top-layer thickness (thus yielding a two-layer system), neutral stability is again obtained. It is clear, however, that this limit has some singular characteristics, as can be seen by the comparison of the curves in Figs. 2 and 3. Similar behavior is seen for cases where the middle-layer or bottom-layer thicknesses become small as well. For the case of density stratification shown in Fig. 6, it is also clear that for cases of density stratification, the lines $R_1 = 1$ and $R_3 = 1$ are both neutrally stable in agreement with the results of Kao.[5] Figure 6 shows that as the middle-layer thickness decreases, the width of the region of instability decreases, and in the limit, neutral stability is obtained.

The value of L in (8a) is seen to characterize whether or not instabilities will be found in the zeroth-order approximation in wave number. The regions of instability in the zeroth-order approximation correspond to parameter values leading to $L > 0$, while the neutrally stable regions in the zeroth-order approximation are characterized by $L < 0$. The previous work of Akhtaruzzaman *et al.*,[7] who consider the zeroth-order approximation in wave number (but do not identify unstable regions), and Wang *et al.*,[8] who consider the first-order correction in wave number [i.e., $O(\alpha)$ as $\alpha \to 0$], focuses on parameter values yielding $L < 0$. Wang *et al.*[8] identify instabilities in the first-order correction; thus, it is seen that the stability of the zeroth-order neutrally stable regions reported in this paper can be determined by considering higher-order corrections in wave number.

As pointed out in the Introduction, Taylor[12] identified a resonating instability that was characterized by underlying inviscid flow fields which allowed for a particularly strong interaction between the interface modes. These strong interactions occurred when the phase velocity of forward moving waves along the bottom interface was approximately equal to the phase velocity of backward moving waves along the upper interface (note that the distinction of backward and forward was made by determining the wave speed relative to the underlying velocities in the top and bottom layers, respectively). The instability could then be thought of as a backward moving wave at the upper interface forcing a forward moving wave at the lower interface when the phase velocity of the two waves coincide. It is interesting to note that in a similar way, Fig. 4(c) demonstrates that the unstable mode travels faster than the fluid at the unperturbed bottom interface, while the unstable mode travels slower than fluid at the unperturbed upper interface and free surface. Thus, we might view the instability discussed in this paper as arising via the above-described resonance effect.

We take this opportunity to further reinforce the comments made by Loewenhurz and Lawrence[9] regarding the identification of a specific wave mode with a particular interface or free surface. They comment that although each mode of solution owes its *existence* to the presence of an interface of free surface, the *whole* perturbation flow field affects each mode. Consequently, the identification of a particular mode with a particular interface can lead to the incorrect interpretation that the mode behavior is not a function of the total flow field and can be attributed totally to local mechanisms. The results in Fig. 4(b) show that despite the fact that it is the interface modes which exhibit the instability, the free surface is largely affected by the interface mode over a large range of E_1. Furthermore, the existence of complex conjugate behavior (which characterizes the instability) necessarily indicates that there is a strong interaction between interfacial modes; these modes must interact through the flow field itself and clearly cannot solely arise due to local mechanisms.

We close this paper by noting that the instability regions in Figs. 2, 3, 5, and 6 afford a smooth transition between regions in the parameter space where interfaces and the free surface have different relative phases; Fig. 4(a) shows a typical example. In their paper, Akhtaruzzaman *et al.*[7] report that the interface and free-surface modes can be in phase or out of phase with one another, depending upon the fluid properties and layer thicknesses. For the range of parameters they consider, they demonstrate that the transition from in-phase to out-of-phase solutions can occur through interface solutions that are completely flat. This type of transition can occur in the neutrally stable regions of the parameter space. The results of this work indicate that over a very broad region of the parameter space, however, transitions in relative phases can *also* occur via a region of instability characterized by conjugate interface modes which yield interface solutions that are *not* flat [as indicated by the relative amplitudes in Fig. 4(b)].

V. CONCLUSIONS

This paper has described a long-wavelength instability which has not previously been identified for three-layer free-surface flow down an inclined plane. The instability is identified in the zeroth-order asymptotic solution in wave number, indicating that *neither* inertial nor finite wavelength effects are necessary to induce instabilities in three-layer systems. Various neutral stability boundaries have been presented which demonstrate the effect of viscosity stratification, density stratification, and layer thicknesses. Our results indicate that destabilization occurs in cases where the middle-layer viscosity (for equal densities in each layer) or density (for equal viscosities in each layer) is smaller than those of the adjacent layers. The regions

of instability afford a smooth transition between neutrally stable regions of the parameter space where the in-phase and out-of-phase characteristics of the interfaces differ.

APPENDIX: SOLUTION OF THE LONG-WAVELENGTH EIGENVALUE PROBLEM

In this appendix, we consider the solution to the system (4), where the goal is to obtain the characteristic equation to solve for c_0, the complex wave speed, as parametrized by (5). The algebra involved can be simplified somewhat by considering cases where there is viscosity stratification but no density stratification ($R_1 = R_3 = 1$), and cases where there is density stratification but no viscosity stratification ($E_1 = E_3 = 1$). For either situation, the solution of (4a) yields:

$$\phi_k(\bar{y}) = F_k\bar{y}^3 + G_k\bar{y}^2 + H_k\bar{y} + I_k, \quad k\in[1,3], \tag{A1}$$

where the F_k, G_k, H_k, and I_k are 12 unknown constants, and it is understood that they are different for the two cases. By inspection, the system (4) provides 12 homogeneous boundary conditions that are used to find nontrivial solutions to the eigenvalue system, i.e., to determine the eigenvalue c_0. The algebra to obtain the characteristic equation for c_0 is entirely straightforward but tedious. The details of the calculation are omitted for this reason, and only the coefficients of the characteristic equation (7) are given in what follows.

Coefficients for the case of viscosity stratification ($R_1 = R_3 = 1$):

$$a_0 = \frac{1}{E_1}\left[S_1(\delta_1^2 - \delta_1^3)\overline{V}_{x_2} + \delta_3\gamma_2\overline{V}_{x_1} - \delta_3\gamma_3\right] - \left(\frac{1}{E_3} + \frac{1}{E_1}(\gamma_1 + \gamma_4)\right)\overline{V}_{x_1}\overline{V}_{x_2} - \overline{V}_{x_1}\overline{V}_{x_2}\overline{V}_{x_3}, \tag{A2a}$$

$$a_1 = -\frac{1}{E_1}[S_1(\delta_1^2 - \delta_1^3) + \delta_3\gamma_2] + \left(\frac{1}{E_3} + \frac{1}{E_1}(\gamma_1 + \gamma_4)\right)(\overline{V}_{x_1} + \overline{V}_{x_2}) + \overline{V}_{x_1}\overline{V}_{x_2} + \overline{V}_{x_3}(\overline{V}_{x_1} + \overline{V}_{x_2}), \tag{A2b}$$

$$a_2 = [(1/E_3) + (1/E_1)(\gamma_1 + \gamma_4)] - (V_{x_1} + \overline{V}_{x_2} + \overline{V}_{x_3}), \tag{A2c}$$

where

$$\gamma_1 = 2\delta_1(1 - E_1) + 2E_1(1 - \delta_3)(1 - 1/E_3), \tag{A2d}$$

$$\gamma_2 = S_2[2\delta_1(1 - E_1)(1 - \delta_3) - \delta_1^2(1 - E_1) + E_1(1 - \delta_3)^2], \tag{A2e}$$

$$\gamma_3 = S_1S_2[\delta_1^2(1 - \delta_3) - \delta_1^3], \tag{A2f}$$

$$\gamma_4 = (1 - \delta_3)^2E_1(1 - 1/E_3) + (1 - E_1) \times [2\delta_1(1 - \delta_3) - \delta_1^2] - (1 - \delta_3)\gamma_1, \tag{A2g}$$

and

$$\overline{V}_{x_1} = -(1/E_1)(\delta_1^2 - 2\delta_1) + D_1, \tag{A3a}$$

$$\overline{V}_{x_2} = 2(1 - \delta_3) - (1 - \delta_3)^2 + D_2, \tag{A3b}$$

$$\overline{V}_{x_3} = (1/E_3) + D_3, \tag{A3c}$$

$$S_1 = 2(1 - \delta_1)(1/E_1 - 1), \tag{A3d}$$

$$S_2 = 2\delta_3(1 - 1/E_3). \tag{A3e}$$

In (A3a)–(A3c), $\overline{V}_{x_1}$, $\overline{V}_{x_2}$, and $\overline{V}_{x_3}$ are the unperturbed fluid velocities at the interface closest to the wall, the second interface, and the free surface, respectively. The jump in rate of strain across the interface closest to the wall is denoted by S_1 in (A3d); S_2 is the jump in strain across the next interface, given in (A3e). Definitions for all additional parameters and constants are given in (1), with $R_1 = R_3 = 1$.

Coefficients for the case of density stratification ($E_1 = E_3 = 1$):

$$a_0 = -\{\delta_1^2(R_1 - 1)\overline{V}_{x_2}\overline{V}_{x_3} + (1 - \delta_3)^2(1 - R_3)\overline{V}_{x_1}\overline{V}_{x_3}\} - R_3(\gamma_4 - \gamma_3\overline{V}_{x_1} + \overline{V}_{x_1}\overline{V}_{x_2} - \gamma_2\overline{V}_{x_2}) - \gamma_1\overline{V}_{x_3} - \overline{V}_{x_1}\overline{V}_{x_2}\overline{V}_{x_3}, \tag{A4a}$$

$$a_1 = -[\delta_1^2(1 - R_1)(\overline{V}_{x_2} + \overline{V}_{x_3}) - (1 - \delta_3)^2(1 - R_3)(\overline{V}_{x_1} + \overline{V}_{x_3})] - R_3[\gamma_2 + \gamma_3 - (\overline{V}_{x_1} + \overline{V}_{x_2})] + \gamma_1 + \overline{V}_{x_1}\overline{V}_{x_2} + \overline{V}_{x_3}(\overline{V}_{x_1} + \overline{V}_{x_2}), \tag{A4b}$$

$$a_2 = -[(R_1 - 1)\delta_1^2 + (1 - \delta_3)^2(1 - R_3) + R_3] - (\overline{V}_{x_1} + \overline{V}_{x_2} + \overline{V}_{x_3}), \tag{A4c}$$

where

$$\gamma_1 = (R_1 - 1)(1 - R_3) \times [\delta_1^2(1 - \delta_3)^2 - 2\delta_1^3(1 - \delta_3) + \delta_1^4], \tag{A4d}$$

$$\gamma_2 = (1 - R_1)(\delta_1^2 - 2\delta_1^3 + \delta_1^4), \tag{A4e}$$

$$\gamma_3 = (R_3 - 1)[(1 - \delta_3)^2 - 2(1 - \delta_3)^3 + (1 - \delta_3)^4], \tag{A4f}$$

$$\gamma_4 = \gamma_1[1 - 2(1 - \delta_3) + (1 - \delta_3)^2], \tag{A4g}$$

and

$$\overline{V}_{x_1} = -R_1\delta_1^2 + C_1\delta_1 + D_1, \tag{A5a}$$

$$\overline{V}_{x_2} = -(1 - \delta_3)^2 - C_2(1 - \delta_3) + D_2, \tag{A5b}$$

$$\overline{V}_{x_3} = -R_3 + C_3 + D_3. \tag{A5c}$$

In (A5a)–(A5c), $\overline{V}_{x_1}$, $\overline{V}_{x_2}$, and $\overline{V}_{x_3}$ are the unperturbed fluid velocities at the interface closest to the wall, the second interface, and the free surface, respectively. Definitions for all additional parameters and constants are given in (1), with $E_1 = E_3 = 1$.

[1]T. B. Benjamin, J. Fluid Mech. **2**, 554 (1957).
[2]A. M. Binnie, J. Fluid Mech **2**, 551 (1957).
[3]C.-S. Yih, Phys. Fluids **6**, 321 (1963).
[4]T. W. Kao, Phys. Fluids **8**, 812 (1965).
[5]T. W. Kao, Phys. Fluids **8**, 2190 (1965).
[6]T. W. Kao, J. Fluid Mech. **33**, 561 (1968).
[7]A. F. M. Akhtaruzzaman, C. K. Wang, and S. P. Lin, ASME J. Appl. Mech. **45**, 25 (1978).
[8]C. K. Wang, J. J. Seaborg, and S. P. Lin, Phys. Fluids **21**, 1669 (1978).
[9]D. S. Loewenhurz and C. J. Lawrence, Phys. Fluids A **1**, 1686 (1989).
[10]S. J. Weinstein, AIChE J. **36**, 1873 (1990).
[11]C. H. Li, Phys. Fluids **12**, 2473 (1969).
[12]G. I. Taylor, Proc. R. Soc. London Ser. A **132**, 499 (1931).
[13]S. P. Lin, J. Fluids Eng. **105**, 119 (1983).
[14]M. Gaster, J. Fluid Mech. **14**, 222 (1962).